Supplementary Information (SI) for EES Solar.
This journal is © The Royal Society of Chemistry 2026

A new era in solar fuels: battery pushes PV-driven CO_2 reduction beyond its limits

Thérèse Cibaka[a,d], Tsvetelina Merdzhanova[a*], Oleksandr Astakhov[a], Robert Zandonella[b], Sergey Shcherbachenko[a,c], Paul Paciok[b], Marc Heggen[b], Rafal Dunin-Borkowski[b], Christoph Brabec[a], Peter Strasser[d]

(a) *Forschungszentrum Jülich GmbH, IMD-3 Photovoltaik, Jülich, Germany.*
(b) *Forschungszentrum Jülich GmbH, Ernst Ruska-Centre, Jülich, Germany.*
(c) *Jülich Aachen Research Alliance (JARA-Energy) and Faculty of Electrical Engineering and Information Technology, RWTH Aachen University, Aachen, Germany.*
(d) *Technical University of Berlin, Institute of Chemistry, Berlin, Germany*

* *t.merdzhanova@fz-juelich.de*

Supplementary information

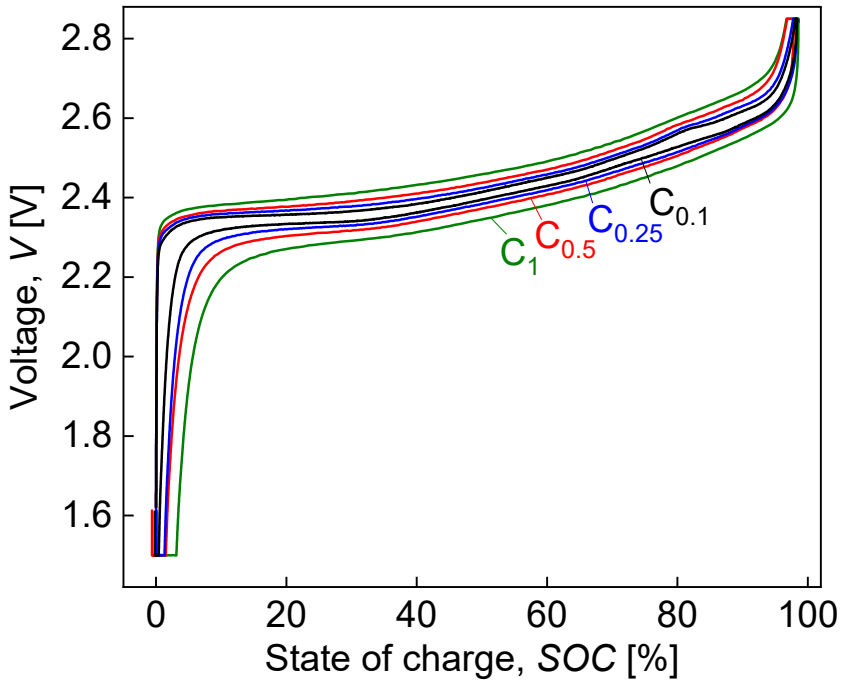

Figure S1. Charge-discharge curves of the Li-ion Battery at C1, C0.5, C0.25 and C0.1.

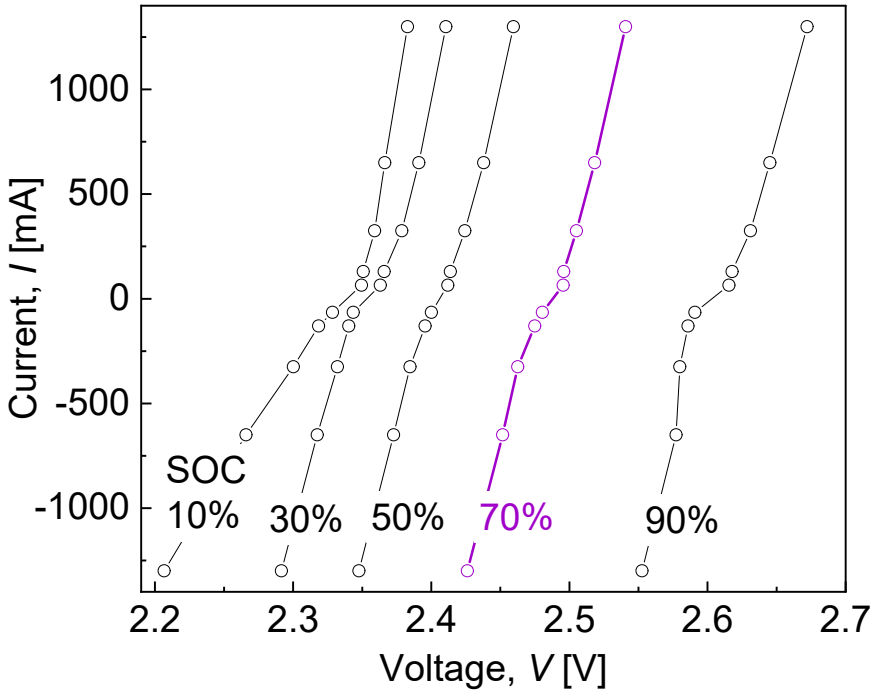

Figure S2 Current-Voltage curves of the Li-ion Battery at state-of-charge 10%, 30%, 50% 70% and 90%

Preparation of Silver gas diffusion electrode

The catalyst ink was an ultrasonication-based dispersion of silver catalyst powder (IoLiTec, 50-60 nm, 99.9 %), nafion (Quintech), isopropanol (Sigma Aldrich, AR) and water (MilliporeSigma, Mili-Q®, IQ7000, 18.2 MΩ.cm). Gas diffusion electrodes (GDE) were fabricated by air-spraying the catalyst ink with a load of approximately 1.5 mg/cm^{-2} to 2 mg/cm^{-2} on cut GDLs (Freudenberg, H23C2) with area of 9.5 cm^2. During the catalyst deposition, the GDL were maintained and dried on a heating plate at 60°C to allow fast evaporation of water and isopropanol.

Electrochemical cell

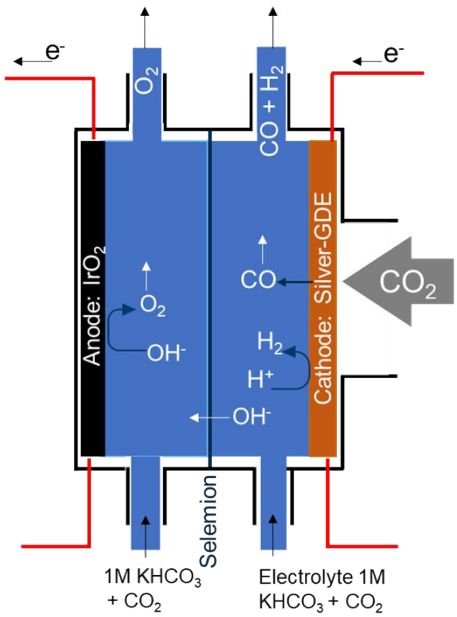

Figure S3. Electrochemical flow-cell consisting of cathode (Silver-GDE), anode (IrO2) and Selemion - anion exchange membrane separating both electrodes. Electrolyte is CO_2-saturated 1M $KHCO_3$ electrolyte. CO2 reduction and oxygen evolution take place at cathode and anode respectively.

Representative Irradiance and Temperature Profiles for PV Emulation

Table S1. Hypothetical summer day simulated in terms of irradiance and module temperature combinations

	Irradiance, sun	Temperature, °C
Morning	0.2	20
	0.4	27
	0.6	34
	0.8	42.8
Noon	1.0	49.8
	1.1	53.3
	1.0	53.3
Afternoon	0.8	49.8
	0.6	42.8
	0.4	35.8
	0.2	28.8

System efficiency evaluation

PV-EC and PV-B-EC systems efficiency are evaluated and compared in terms of solar-to-chemicals (*STC*) efficiency and coupling factor.

PV-EC

For PV-EC operation, the STC is determined by multiplying the efficiency of the PV system (ηPV), the PV-EC coupling efficiency (C), and the efficiency of the electrochemical conversion (ηEC), as shown in equations (3 - 10) below. The PV efficiency represents the proportion of incident solar power on the exposed surface of the photovoltaic system that is converted into electrical power at the maximum power point.

$$\eta_{PV} = \frac{V_{MPP} I_{MPP}}{A_{PV} G} = \frac{P_{MPP}}{A_{PV} G} \quad (3),$$

where V_{MPP}, I_{MPP} and P_{MPP} are voltage, current and power of PV at the maximum power point, A_{PV} is the exposed area of PV module and G is solar irradiance.

PV-EC power coupling efficiency defines the fraction of the maximum power that the PV system can deliver which is effectively used by the electrochemical process at the operating point.

$$C = \frac{V_{OP} I_{OP}}{V_{MPP} I_{MPP}} \quad (4),$$

Where V_{OP} and I_{OP} are voltage and current of EC at the operating point. To obtain operating current density J_{OP}, I_{OP} is divided by the area of EC, 9.5 cm^2.

PV-EC energy coupling efficiency represents how much of the maximum energy deliverable by PV is actually being utilized by EC during operating time.

$$C = \frac{\int V_{OP} I_{OP}}{\int V_{MPP} I_{MPP}} = \frac{E_{OP}}{E_{MPP}} \quad (5)$$

Faradaic efficiency (or selectivity), FE_p, of a chemical product evaluates which fraction of the operating current (I_{OP}) is utilized for the formation of that specific chemical (H_2 or CO),

$$FE_p = \frac{n \times x_p \times F \times CO_2\, flowrate}{I_{OP}} \quad (6),$$

Where n is the number of electrons required to obtain one molecule of the specific chemical (CO or H_2), x_p is the concentration of that chemical in ppm, F is the faradaic constant (96485 C/mol).

EC efficiency for a specific product (η_{ECp}) is determined by the product of faradaic efficiency and voltage efficiency for that particular chemical. η_{ECp} represents the proportion of the operating power (voltage and current) effectively utilized for the production of the specific chemical (Equation 7).

$$\eta_{ECp} = \frac{FE_p E_p^0}{V_{OP}} \quad (7),$$

Where *Ep°* is the thermoneutral voltage for thatc chemical, E° is 1.47V for H_2 and CO.

The overall EC efficiency η_{EC}, is the sum of all $\eta_{ECp.}$

$$\eta_{EC} = \sum \eta_{ECp} \quad (8),$$

STC towards individual product is STC_p and *STC* towards all products.

$$STC_p = \eta_{PV}\, C\, \eta_{ECp} \quad (9)$$

$$STC = \eta_{PV}\, C\, \eta_{EC} \quad (10)$$

The EC cell used in our work produced CO and H_2 therefore we estimate *STC* (H2) and *STC* (CO) for both of the products as well as the total *STC* as their sum.

PV-B-EC

The PV conversion efficiency is obtained with Equation 1,

The power coupling factor for PV-B-EC, C^*, is calculated with equation (11)

$$C^* = \frac{V_{OP*} I_{OP*}}{V_{MPP} I_{MPP}} \quad (11)$$

V_{OP*} and I_{OP*} represent the operating current and voltage of the joint B-EC directly connected to PV.

PV-B-EC energy coupling efficiency represents how much of the maximum energy deliverable by PV is actually being utilized by battery and EC during daytime.

$$C = \frac{\int V_{OP*} I_{OP*}}{\int V_{MPP} I_{MPP}} = \frac{E_{OP*}}{E_{MPP}} \quad (12)$$

EC power efficiency for a specific product (η_{EC}) is determined by the product of faradaic efficiency and voltage efficiency for that particular chemical. η_{ECp} represents the proportion of the operating power (voltage and current) effectively utilized for the production of the specified chemical (Equation 13).

$$\eta_{EC} = \sum \eta_{ECp} = \frac{FE_{CO} E_{CO}^{0}}{V_{OP}} + \frac{FE_{H2} E_{H2}^{0}}{V_{OP}} \quad (13),$$

Faradaic efficiency of each product (CO and H_2) is obtained with equation (14)

$$FE_p = \frac{n \times x_p \times F \times CO_2\, flowrate}{I_{EC(day\ or\ night)}} \quad (14)$$

Voltage efficiency is determined by equation (15)

$$\eta_{VEC} = \frac{E_{CO}^{0}}{V_{OP}} + \frac{E_{H2}^{0}}{V_{OP}} \quad (15)$$

In PV-B-EC operation, solar-to-chemical efficiency (STC) can only be evaluated as the ratio between cumulative solar energy incident on the exposed PV area during daytime to the cumulative chemical energy stored in the products (CO and H_2) generated by the EC during both day- and night-time operation. The cumulative sun energy is calculated with equation (16).

$$E_{sun} = \int_{0}^{t_{day}} G_t\, A_{PV}\, dt \quad (16)$$

Where t_{day} is the duration of the simulated "day".

The cumulative energy involved in chemicals formation are obtained with equations (17)-(19).

$$E_{CO+H2}\,(day) = \int_{0}^{t_{day}} E_{CO}^{0}\ FE_{CO}\, I_{EC}\, dt \ + \int_{0}^{t_{day}} E_{H2}^{0}\ FE_{H2}\, I_{EC}\ dt \quad (17)$$

$$E_{CO+H2}\,(night) = \int_{t_{day}}^{t_{night}} E_{CO}^{0}\ FE_{CO}\, I_{EC}\, dt + \int_{t_{day}}^{t_{night}} E_{H2}^{0}\ FE_{H2}\, I_{EC}\, dt \quad (18)$$

$$E_{CO+H2} = E_{CO+H2}(day) + E_{CO+H2}(night) \quad (19)$$

Where t_{day} is the duration of daytime; t_{night} is the duration of the night required for all the PV energy stored in the battery during the day to be fully utilized by the electrochemical cell.

Solar to chemical efficiency is, then, calculated with equation (18)

$$STC = E_{CO+H2}/E_{sun} \quad (18)$$

Operating power of EC in PV-EC configuration in comparison with PV-B-EC

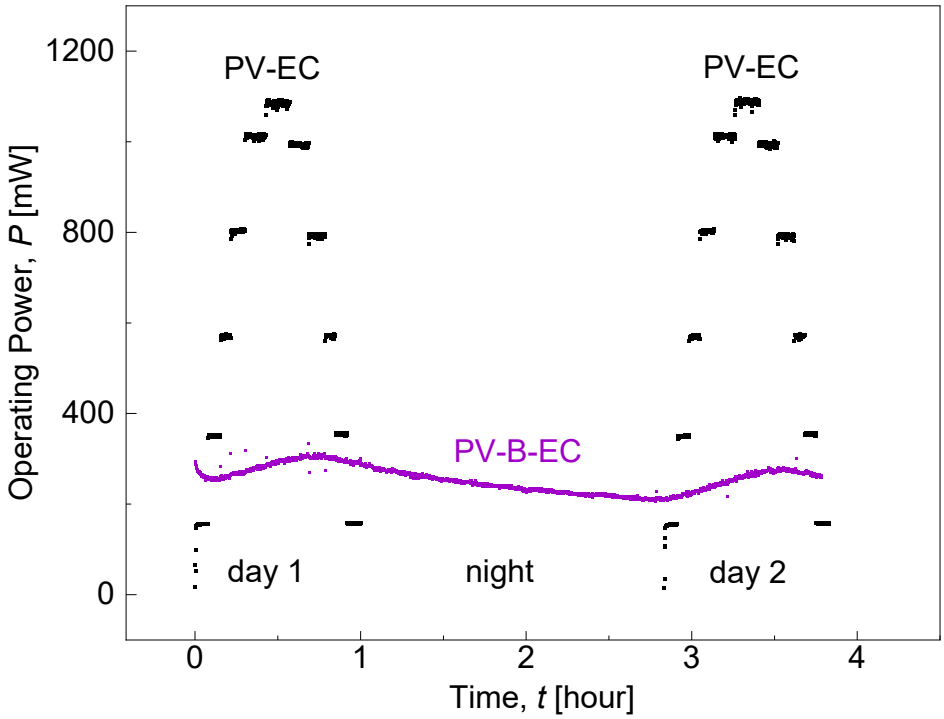

Figure S4. Comparison of electrochemical cell's operating power in PV-EC and PV-B-EC configuration.

Microstructural analysis of Ag nanoparticles under fluctuating versus under constant voltage

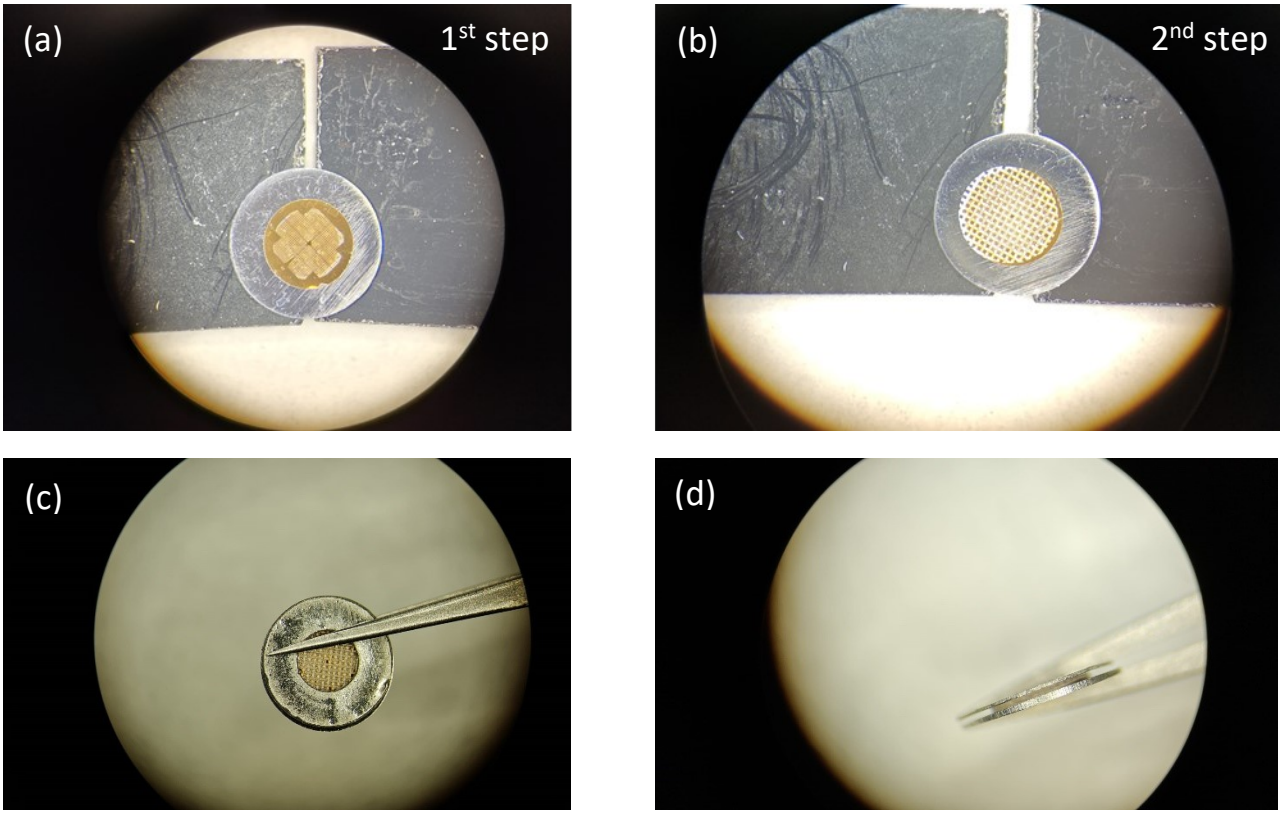

Figure S5. The fabrication procedure of Ag TEM-grid cathodes with 1st step: Ag-containing finder grid laying on the Plasma-cleaned ring and 2nd step: Nylon grid covering Ag-containing finder grid and another plasma-cleaned ring to close the sandwich-like setup. (a) Front view of inverted tweezer holding Ag TEM-grid cathode. (b) Side view of inverted tweezer holding Ag TEM-grid cathode.

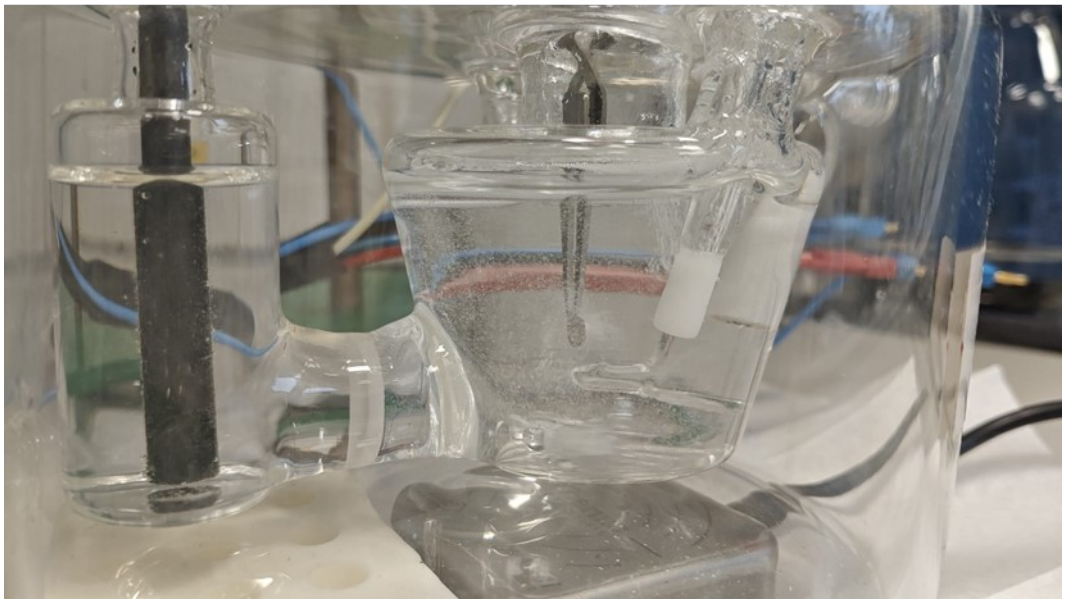

Figure S6. Close-up of electrodes in custom-made H-cell operating with 1M $KHCO_3$ at approximately 25°C, the experimental setup for CO_2 reduction used TEM-grid deposited with Ag as cathode and graphite rod as counter electrode

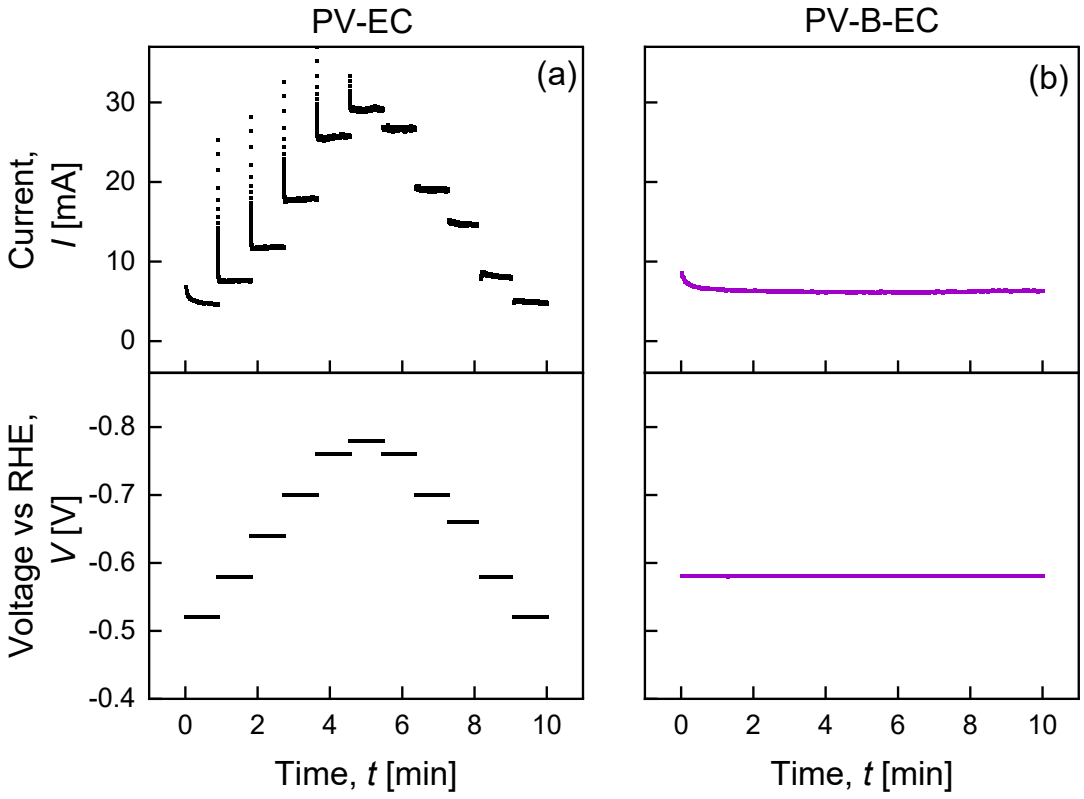

Figure S7. current-voltage behaviors of TEM grid deposited with Ag as cathode (a) Fluctuating operating voltage simulating PV-EC scenario (b) Constant operating voltage of -0.58V simulating PV-B-EC configuration.

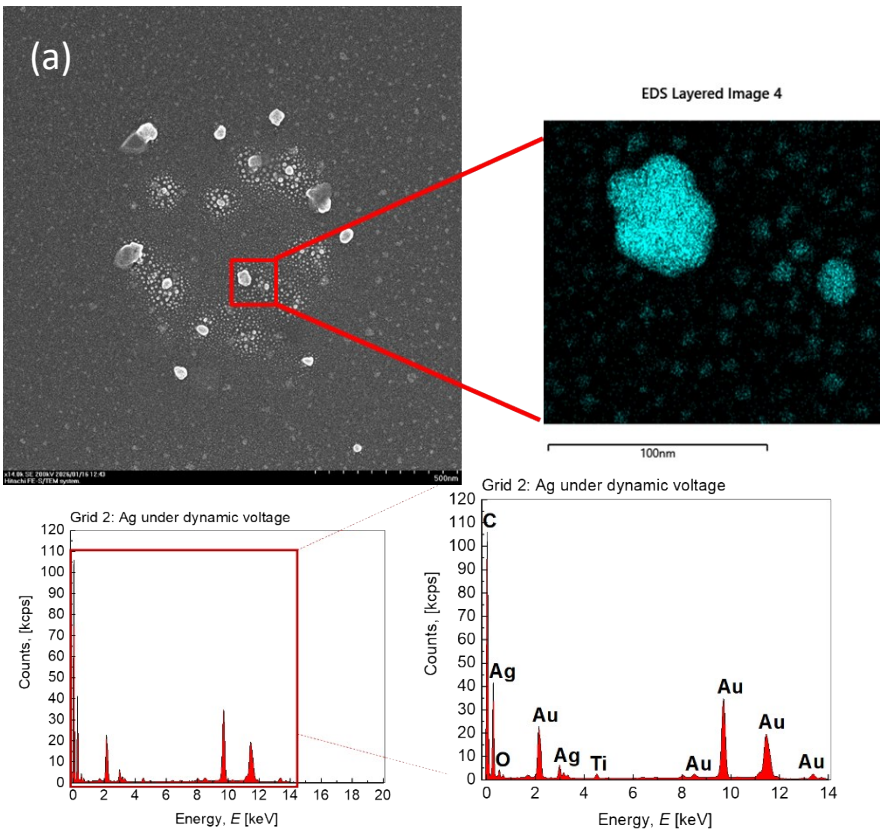
(a)
EDS Layered Image 4
100nm
Grid 2: Ag under dynamic voltage
Counts, [kcps]
Energy, E [keV]
Grid 2: Ag under dynamic voltage
C
Ag
Au
O
Ag
Ti
Au
Au
Au
Counts, [kcps]
Energy, E [keV]

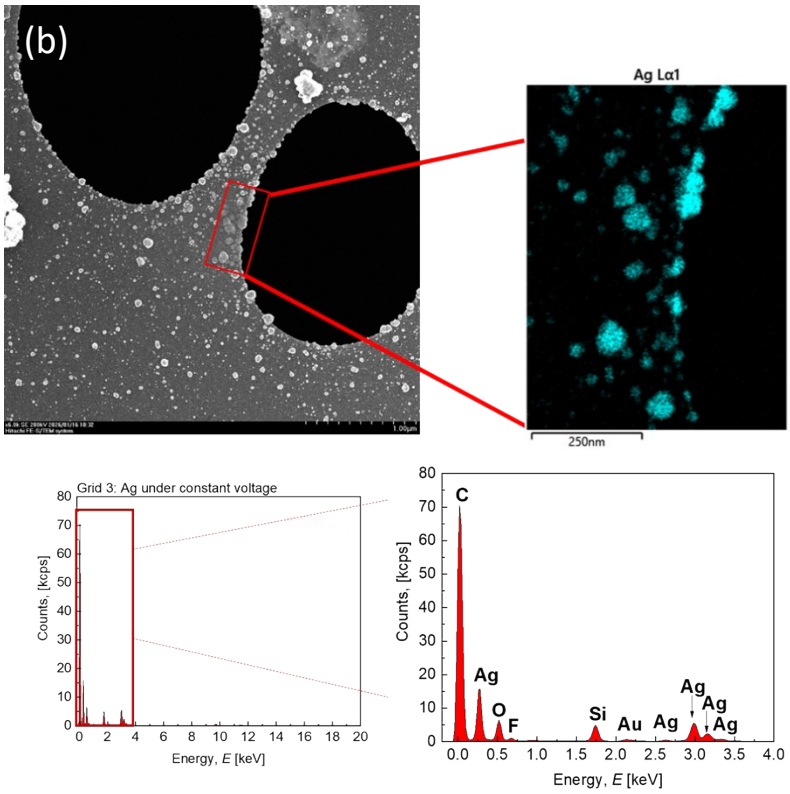
(b)
Ag Lα1
250nm
Grid 3: Ag under constant voltage
Counts, [kcps]
Energy, E [keV]
C
Ag
O
F
Si
Au
Ag
Ag
Ag
Ag
Counts, [kcps]
Energy, E [keV]

167

Figure S8. Secondary electron images (left) of small particle aggregates. The regions highlighted by red squares were analyzed by energy-dispersive X-ray spectroscopy (EDX), with the corresponding EDX spectra and silver elemental maps shown on the right. (a) Grid 2: Ag after electrolysis under a dynamic voltage profile. (b) Grid 3: Ag after electrolysis under a constant voltage profile.

Analysis of the results, synergy in B-EC operation and efficiency beyond the limit

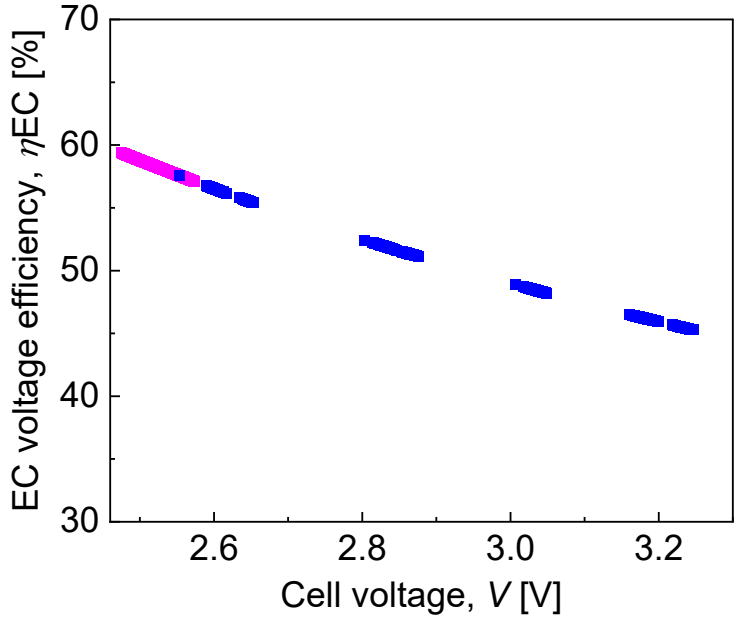

Figure S9. Hyperbolic dependence of EC voltage efficiency with EC voltage

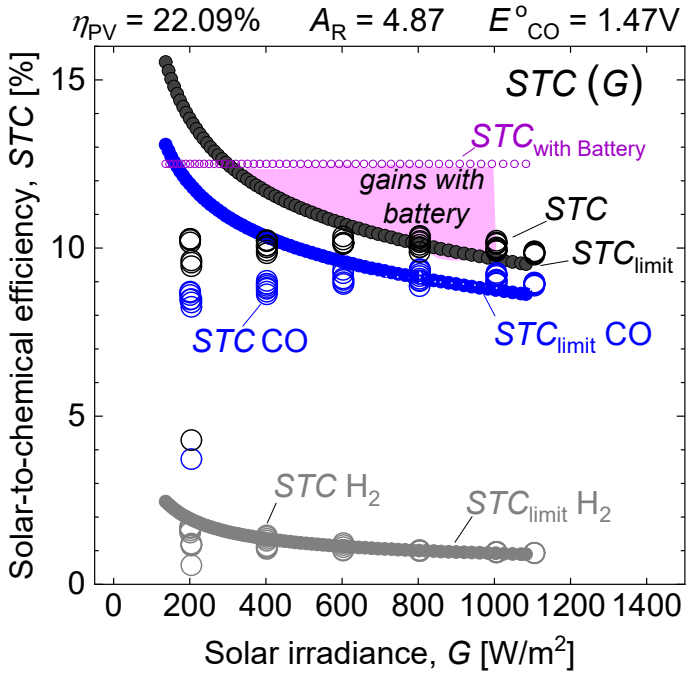

Figure S10. Comparison of theoretical solar-to-chemical efficiency limit STC_{limit} calculated for our EC using η_{PV} = 22.09% and PV-to-EC area ratio A_R= 4.87 with the measured solar-to-chemical efficiencies of the PV-EC system. STC_{limit} are presented as filled circles (black: CO+H_2, blue: CO, grey: H_2), while the experimentally measured STC values for the PV-EC configuration are shown as hollow circles in the same color scheme. The measured STC values for the PV-B-EC device are displayed as pink hollow circles and exceed the STC_{limit} attainable by the PV-EC reference system.

179